arXiv:1011.1597v1 [cond-mat.mtrl-sci] 6 Nov 2010

Entropic Effect on the Rate of Dislocation Nucleation

Seunghwa Ryu[1*], Keonwook Kang[2] and Wei Cai[2]

[1]*Department of Physics, Stanford University, Stanford, California 94305*

[2]*Department of Mechanical Engineering,*

Stanford University, Stanford, California 94305

Abstract

Dislocation nucleation is essential to our understanding of plastic deformation, ductility and mechanical strength of crystalline materials. Molecular dynamics simulation has played an important role in uncovering the fundamental mechanisms of dislocation nucleation, but its limited time scale remains a significant challenge for studying nucleation at experimentally relevant conditions. Here we show that dislocation nucleation rates can be accurately predicted over a wide range of conditions by determining the activation free energy from umbrella sampling. Our data reveal very large activation entropies, which contribute a multiplicative factor of many orders of magnitude to the nucleation rate. The activation entropy at constant strain is caused by thermal expansion, with negligible contribution from the vibrational entropy. The activation entropy at constant stress is significant larger than that at constant strain, as a result of thermal softening. The large activation entropies are caused by anharmonic effects, showing the limitations of the harmonic approximation widely used in solids. Similar behaviors are expected to occur in other nucleation processes in solids.

* corresponding author:shryu@stanford.edu

Nucleation plays an important role in a wide range of physical, chemical and biological processes [1–6]. In the last two decades, the nucleation of dislocations in crystalline solids has attracted significant attention, not only for the reliability of microelectronic devices [7], but also as a responsible mechanism for incipient plasticity in nano-materials [8–10] and nano-indentation [11–13]. However, predicting the nucleation rate as a function of temperature and stress from fundamental physics is extremely difficult. Because the critical nucleus can be as small as a few lattice spacings, the applicability of continuum theory [14] becomes questionable. At the same time, the time scale of molecular dynamics (MD) simulations is about ten orders of magnitude smaller than the experimental time scale. Hence MD simulations of dislocation nucleation are limited to conditions at which the nucleation rate is extremely high [15, 16].

One way to predict dislocation nucleation rate under common experimental loading rates [17] is to combine the transition state theory (TST) [5, 18] and the nudged-elastic-band (NEB) method [19]. TST predicts that the nucleation rate per nucleation site in a crystal subjected to constant strain γ can be written as

$$I^{\mathrm{TST}} = \nu_0 \exp\left[-\frac{F_c(T,\gamma)}{k_B T}\right] \tag{1}$$

where F_c is the activation free energy, T is temperature, and k_B is Boltzmann's constant. $\nu_0 = k_B T/h$ is the frequency prefactor, where h is Planck's constant. Note that $F_c(T,\gamma) = E_c(\gamma) - TS_c(\gamma)$, where E_c and S_c are the activation energy and activation entropy, respectively. Here we assume the dependence of E_c and S_c on T is weak, which is later confirmed numerically. For a crystal subjected to constant stress σ, $F_c(T,\gamma)$ in Eq. (1) should be replaced by the activation Gibbs free energy $G_c(T,\sigma) = H_c(\sigma) - TS_c(\sigma)$, where H_c is the activation enthalpy. Because the NEB method only computes the activation energy, the contribution of S_c is often ignored in rate estimates in solids. Recently, an approximation of $S_c(\sigma) = H_c(\sigma)/T_m$ is used [17], where T_m is the surface disordering temperature. This approximation was questioned by subsequent MD simulations [20]. The magnitude of S_c remains unknown due to the lack of a method to compute it accurately over a wide range of temperature and stress conditions.

We successfully applied the umbrella sampling [21] method to compute the activation free energy for homogeneous and heterogeneous dislocation nucleation in copper. Based on this input, the nucleation rate is predicted using the Becker-Döring theory [22]. Comparison

with direct MD simulations at high stress confirms the accuracy of this approach. Both $F_c(T,\gamma)$ and $G_c(T,\sigma)$ show significant reduction with increasing T, corresponding to large activation entropies. For example, $S_c(\gamma = 0.092) = 9\,k_B$ and $S_c(\sigma = 2\,\mathrm{GPa}) = 48\,k_B$ are observed in homogeneous nucleation. We found that $S_c(\gamma)$ is caused by the anharmonic effect of thermal expansion, with negligible contribution from the vibrational entropy. The large difference in the two activation entropies, $\Delta S_c \equiv S_c(\sigma) - S_c(\gamma)$, is caused by thermal softening, which is another anharmonic effect. Similar behaviors are expected to occur in other nucleation processes in solids.

For simplicity, we begin with the case of homogeneous dislocation nucleation in the bulk. Even though dislocations often nucleate heterogeneously at surfaces or internal interfaces, homogeneous nucleation is believed to occur in nano-indentation [11] and in a model of brittle-ductile transition [23]. It also provides an upper bound to the ideal strength of the crystal. Our model system is a copper single crystal described by the embedded-atom method (EAM) potential [24]. As shown in Fig. 1(a), the simulation cell is subjected to a pure shear stress along $[11\overline{2}]$. The dislocation to be nucleated lies on the (111) plane and has the Burgers vector of a Shockley partial [25], $\mathbf{b}_p = [11\overline{2}]/6$. Fig. 1(b) shows the shear stress-strain relationship of the perfect crystal at different temperatures (before dislocation nucleation).

In this work, we predict the nucleation rate based on the Becker-Döring (BD) theory, which expresses the nucleation rate per nucleation site as,

$$I^{\mathrm{BD}} = f_c^+ \,\Gamma\, \exp\left[-\frac{F_c(T,\gamma)}{k_B T}\right] \tag{2}$$

where f_c^+ is the molecular attachment rate, and Γ is the Zeldovich factor (see Methods). The BD theory and TST only differs in the frequency prefactor. While TST neglects multiple recrossing over the saddle point by a single transition trajectory [5], this is accounted for in the BD theory through the Zeldovich factor.

First, we establish the validity of the BD theory for dislocation nucleation by comparing it against direct MD simulations at a relatively high stress $\sigma = 2.16$ GPa ($\gamma = 0.135$) at $T = 300$K, which predicts $I^{\mathrm{MD}} = 2.5 \times 10^8\,\mathrm{s}^{-1}$ (see Methods). The key input to the BD theory is the activation Helmholtz free energy $F_c(T,\gamma)$, which is computed by umbrella sampling. The umbrella sampling is performed in Monte Carlo simulations using a bias potential as a function of the order parameter n, which is chosen as the number of atoms

inside the dislocation loop (see Methods).

Fig. 2(a) shows the free energy function $F(n)$ obtained from umbrella sampling for the specified (T, γ) condition. The maximum of $F(n)$ gives the activation free energy $F_c = 0.527 \pm 0.001$ eV and the critical nucleus size $n_c = 36$. The Zeldovich factor [28], $\Gamma = 0.055$, is obtained from $\Gamma \equiv \left(\frac{\eta}{2\pi k_B T}\right)^{1/2}$ where $\eta = -\partial^2 F(n)/\partial n^2|_{n=n_c}$.

Using the configurations collected from umbrella sampling with $n = n_c$ as initial conditions, MD simulations give the attachment rate $f_c^+ = 5.3 \times 10^{14}\,\mathrm{s}^{-1}$ (see Methods). Because the entire crystal is subjected to uniform stress, the number of nucleation sites is the total number of atoms, $N_{\mathrm{atom}} = 14976$. Combining these data, the Becker-Döring theory predicts the total nucleation rate to be $N_{\mathrm{atom}} I^{\mathrm{BD}} = 6.2 \times 10^8\,\mathrm{s}^{-1}$. This is within a factor of 3 of the MD prediction and the difference between the two is comparable to our error bar. This agreement shows that the Becker-Döring theory and our numerical approach are suitable for the calculation of dislocation nucleation rate.

We now examine the dislocation nucleation rate under a wide range of temperature and strain (stress) conditions relevant for experiments and beyond the limited time scale of MD simulations. Fig. 3(a) shows the activation Helmholtz free energy $F_c(T, \gamma)$ as a function of γ at different T. The zero temperature data is obtained a minimum-energy-path (MEP) search using a modified version of the string method, similar to that used in [17, 29]. The downward shift of F_c curves with increasing T is the signature of the activation entropy S_c. Fig. 3(c) plots F_c as a function of T at $\gamma = 0.092$. The data closely follow a straight line, whose slope gives $S_c(\gamma) = 9.0\ k_B$. This contributes a significant multiplicative factor, $\exp(S_c/k_B) \approx 10^4$, to the absolute nucleation rate, and cannot be ignored.

What causes this rapid drop of activation free energy with temperature? Thermal expansion and vibrational entropy are two candidate mechanisms. To examine the effect of thermal expansion, we performed zero temperature MEP search at $\gamma = 0.092$, but with other strain components fixed at the equilibrated values at $T = 300$ K. The resulting activation energy, $\tilde{E}_c = 2.04$ eV, is indistinguishable from the activation free energy F_c at $T = 300$ K computed from umbrella sampling. Because atoms do not vibrate in the MEP search, this result shows that the dominant mechanism for the large $S_c(\gamma)$ is thermal expansion, while the contribution from vibrational entropy is negligible. As temperature increases, thermal expansion pushes neighboring atoms further apart and weakens their mutual interaction. This makes crystallographic planes easier to shear and significantly reduces the free

energy barrier for dislocation nucleation. In the widely used harmonic approximation of TST, the activation entropy is often attributed to the vibrational degrees of freedom as $\nu_0 \exp(S_c/k_B) = (\prod_{i=1}^{\mathcal{N}} \nu_i^{\rm m})/(\prod_{i=1}^{\mathcal{N}-1} \nu_i^{\rm a})$, where $\nu_i^{\rm m}$ and $\nu_i^{\rm a}$ are the positive normal frequencies around the local energy minimum and activated state, respectively [5, 18]. However, here we see that $S_c(\gamma)$ arises entirely from the anharmonic effect.

While it is easier to control strain γ than stress σ in atomistic simulations, it is usually easier to apply stress in experiments, and experimental results are often expressed as a function of σ and T. To bridge between simulations and experiments, it is important to establish a connection between the constant-stress and constant-strain ensembles. In the constant-strain ensemble, the system is described by the Helmholtz free energy $F(n, T, \gamma)$ where n is the size of the dislocation loop and the activation Helmholtz free energy is defined as $F_c(T, \gamma) \equiv F(n_c, T, \gamma) - F(n{=}0, T, \gamma)$. In the constant-stress ensemble, the system is described by the Gibbs free energy $G(n, T, \sigma)$, from the Legendre transform $G = F - \sigma\, \gamma\, V$, with $\sigma \equiv V^{-1} \partial F/\partial \gamma|_{n,T}$. Similarly, $G_c(T, \sigma) \equiv G(n_c, T, \sigma) - G(n{=}0, T, \sigma)$. We have proved that $G_c(T, \sigma) = F_c(T, \gamma)$ in the thermodynamic limit of $V \to \infty$, when σ and γ satisfies the stress-strain relation of the perfect crystal, $\sigma(\gamma, T)$. The difference between F_c and G_c when $\sigma = \sigma(T, \gamma)$ is of the order $\mathcal{O}(V^{-1})$. The details of the proof will be published separately.

Combining the activation Helmholtz free energy $F_c(T, \gamma)$ shown in Fig. 3(a) and the stress-strain relations shown in Fig. 1(b), we obtain the activation Gibbs free energy $G_c(T, \sigma)$, which is shown in Fig. 3(b). We immediately notice that the curves at different temperatures are more widely apart in $G_c(T, \sigma)$ than that in $F_c(T, \gamma)$, indicating a much larger activation entropy in the constant-stress ensemble. For example, Fig. 3(d) plots G_c as a function of T at $\sigma = 2.0$ GPa, from which we can obtain an averaged activation entropy of $\overline{S_c}(\sigma) = 48\, k_B$ in the temperature range of $[0, 300\text{K}]$. This contributes a multiplicative factor of $\exp(\overline{S_c}(\sigma)/k_B) \approx 10^{20}$ to the absolute nucleation rate.

The dramatic difference between $S_c(\gamma)$ and $S_c(\sigma)$ may seem surprising. Indeed, they are sometimes used interchangeably [31, 32], although the conceptual difference between the two has been pointed out in the context of chemical reactions [33, 34]. It is well known that the entropy is independent of the ensemble of choice, i.e. $S(n, T, \gamma) \equiv \partial F(n, T, \gamma)/\partial T|_{n,\gamma}$ and $S(n, T, \sigma) \equiv \partial G(n, T, \gamma)/\partial T|_{n,\sigma}$ equal to each other as long as $\sigma = V^{-1} \partial F/\partial \gamma|_{n,T}$, which is true by definition. At the same time, the activation entropy is just the entropy difference between the activated state and the metastable state, i.e. $S_c(T, \gamma) = S(n_c, T, \gamma) - S(n{=}$

$0, T, \gamma)$ and $S_c(T, \sigma) = S(n_c, T, \sigma) - S(n{=}0, T, \sigma)$. If the entropies in two ensembles can equal each other, it may seem puzzling how the activation entropies can be different.

The resolution of this apparent paradox is that under the constant applied stress, the nucleation of a dislocation loop causes a strain increase, i.e. $\sigma(n{=}0, T, \gamma) = \sigma(n_c, T, \gamma^+)$, with $\gamma^+ > \gamma$. Based on this result, one can show that the difference in the activation entropies, $\Delta S_c \equiv S_c(\sigma) - S_c(\gamma)$, equals $S(n{=}0, T, \gamma^+) - S(n{=}0, T, \gamma)$, which is the entropy difference of the perfect crystal at two slightly different strains. We can further show that $\Delta S_c = -\Omega_c(\sigma)\partial\sigma/\partial T|\gamma$, where $\Omega_c \equiv -\partial G_c/\partial\sigma|_T$ is the activation volume and $-\partial\sigma/\partial T|\gamma$ describes the thermal softening effect. Hence ΔS_c is always positive for nucleation processes in solids driven by shear stress. In the case of homogeneous dislocation nucleation ΔS_c as large as $39\,k_B$ is observed for homogeneous dislocation nucleation, which is mainly caused by its large activation volume Ω_c. The numerical results enable us to examine the approximation [17] based on the so-called thermodynamic "compensation law" [30], which states that the activation entropy is proportional to the activation enthalpy (or energy). We find that $S_c(\gamma)$ can be roughly approximated by $E_c(\gamma)/T^*$ with $T^* \approx 3000$ K while $S_c(\sigma)$ can be approximated by $H_c(\sigma)/T^\dagger$ only in the large stress limit, with $T^\dagger \approx 390$ K (see supplementary materials).

To assess the applicability of these conclusions in heterogeneous nucleation, we studied dislocation nucleation from the corner of a [001]-oriented copper nanorod with {100} side surfaces under axial compression (see Methods). Fig. 4(b) plots the activation free energy barrier as a function of axial compressive stress σ, which shows significant reduction of the activation free energy with temperature. For example, at the compressive elastic strain of $\epsilon = 0.03$, the compressive stress is $\sigma = 1.55$ GPa at $T = 0$ K. The activation entropy $S_c(\epsilon)$ at this elastic strain equals $6.9k_B$, whereas the activation entropy $S_c(\sigma)$ at this stress equals $19k_B$. Fig. 4(c) plots the contour lines of the predicted dislocation nucleation rate (per nucleation site) as a function of T and σ. To show the physical effect of the large activation entropies, the dashed lines plot the rate predictions if the effect of $S_c(\sigma)$ were completely neglected. Significant deviations between the two sets of contour lines are observed, especially for $T \geq 300$ K and $\sigma \leq 1.5$ GPa. For example, at $T = 300$ K and $\sigma = 1.5$ GPa (where a thick and a thin contour line cross), the neglect of activation entropy would cause an underestimate of the nucleation rate by 10 orders of magnitude.

In summary, we have shown that the Becker-Döring theory combined with free energy

barriers determined by umbrella sampling can accurately predict the rate of homogeneous dislocation nucleation. In both homogeneous and heterogeneous dislocation nucleation, a large activation entropy at constant elastic strain is observed, and is attributed to the weakening of atomic bonds due to thermal expansion. An even larger activation entropy is observed at constant stress, due to thermal softening. Both effects are anharmonic in nature, and emphasize the need to go beyond harmonic approximation in the application of rate theories in solids. We believe our methods and the general conclusions are applicable to a wide range of nucleation processes in solids that are driven by shear stress, including cross slip, twinning and martensitic phase transformation.

METHODS

Molecular Dynamics

The simulation cell for homogeneous dislocation nucleation has dimension $8[11\overline{2}]\times6[111]\times3[1\overline{1}0]$. Periodic boundary conditions (PBC) are applied to all 3 directions. To reduce artifacts from periodic image interactions, the applied stress is always large enough so that the diameter of critical dislocation loop is smaller than half the width of the simulation cell.

The shear strain γ is the x-y component of the engineering strain. The following procedure is used to obtain pure shear stress-strain curve shown in Fig. 1(b). At each temperature T and shear strain γ_{xy}, a series of 2 ps MD simulations under the NVT ensemble are performed. After each simulation, all strain components except γ_{xy} are adjusted according to the average Virial stress until σ_{xy} is the only non-zero stress component. The shear strain is then increased by 0.01 and the process repeats until the crystal collapses spontaneously. The shear stress-strain data are fitted to a polynomial function, $\sigma(\gamma,T)=\sum_{i=0}^{2}\sum_{j=0}^{2}a_{ij}\gamma^{i}T^{j}$.

To obtain average nucleation time at $\sigma_{xy}=2.16$ GPa ($\gamma=0.135$) at 300 K, we performed 192 independent MD simulations using the NVT ensemble with random initial velocities. Each simulation runs for 4 ns. If dislocation nucleation occurs during this period, the nucleation time is recorded. This information is used to construct the function $P_s(t)$, which is the fraction of MD simulation cells in which dislocation nucleation has not occurred at time t. $P_s(t)$ can be well fitted to the form of $\exp(-I^{\mathrm{MD}}t)$ to extract the nucleation rate I^{MD}.

To compute the attachment rate f_c^+, we collect from umbrella sampling an ensemble of 500 atomic configurations for which $n = n_c$, and run MD simulations using each configuration as an initial condition. The initial velocities are randomized according to Boltzmann's distribution. The mean square change of the loop size, $\langle \Delta n^2(t) \rangle$, as shown in Fig. 2(b), is fitted to a straight line, $2f_c^+ t$, in order to extract f_c^+ [26].

Free energy barrier calculations

The reaction coordinate n is defined for each atomic configurations in the following way. An atom is labelled as "slipped" if its distance from any of its original nearest neighbors has changed by more than the critical distance d_c [27]. $d_c = 0.33$ Å, 0.38 Åand 0.43 Åfor $T \leq 400$ K, $T = 500$ K and $T = 600$ K, respectively. The "slipped" atoms are grouped into clusters; two atoms belong to the same cluster if their distance is less than cutoff distance r_c (3.4 Å). The reaction coordinate n is the number of atoms in the largest cluster divided by two.

To perform umbrella sampling, a bias potential $k_B \hat{T} (n - \overline{n})^2$ is superimposed on the EAM potential, where $\hat{T} = 40$ K and $\overline{n}$ is the center of the sampling window. $\hat{T}$ is empirically chosen so that the width of the sampling window on the n-axis is about 10. The Helmholtz free energy data can be fitted very well by a polynomial function, $F(\gamma, T) = \sum_{i=0}^{2} \sum_{j=0}^{1} b_{ij} \gamma^i T^j$.

For heterogeneous dislocation nucleation, the size of the copper nanorod [17] is $15[100] \times 15[010] \times 20[001]$ with PBC along [001].

ACKNOWLEDGEMENTS

This work is supported by the NSF Grant CMS-0547681 and a DOE SciDAC project on Quantum Simulation of Materials and1 Nanostructures.

AUTHOR CONTRIBUTION

S.R. and W.C. designed the research plan; S.R. and K.K. designed and implemented the method; S.R. carried out the calculations; S.R., K.K. and W.C. analysed the data and wrote the paper.

ADDITIONAL INFORMATION

Supplementary information accompanies this paper on www.nature.com/naturematerials. The authors declare no competing financial interests. Reprints and permissions information is available online at http://npg.nature.com/reprintsandpermissions. Correspondence and requests for materials should be addressed to S. R. (shryu@stanford.edu).

[1] Walsh, M. R., Koh, C. A., Sloan, E. D., Sum, A. K., & Wu, D. T. Microsecond simulations of spontaneous methane hydrate nucleation and growth. Science **326** , 1095-1098 (2009).

[2] Anderson, V. J. & Lekkerkerker, H. N. W. Insights into phase transition kinetics from colloid science. Nature **416**, 811-815 (2002).

[3] Matsumoto, M., Saito, S., & Ohmine, I. Molecular dynamics simulation of the ice nucleation and growth process leading to water freezing. Nature **416**, 409-413 (2002).

[4] Laaksonen, A., Talanquer, V. & Oxtoby, D. W. Nucleation: measurements, theory, and atmospheric applications. Annu. Rev. Phys. Chem. **46**, 489-524 (1995).

[5] Hänggi, P., Talkner, P. & Borkovec, M. Reaction-rate theory: fifty years after Kramers. Rev. Mod. Phys. **62**, 251, (1990).

[6] ten Wolde, P. R. & Frenkel, D. Enhancement of protein crystal nucleation by critical density fluctuations. Science, **277**, 1975-1978 (1997).

[7] Izumi, S., Ohta, H., Takahashi, C., Suzuki, T. & Saka, H. Shuffle-set dislocation nucleation in semiconductor silicon device. Philos. Mag. Lett. **90**, 707-714 (2010).

[8] Li, X., Wei, Y., Lu, L., Lu, K., & Gao, H. Dislocation nucleation governed softening and maximum strength in nano-twinned metals. Nature **464**, 877-880 (2010).

[9] Li, J. The mechanics and physics of defect nucleation. MRS Bull. **32**, 151-159 (2007)

[10] Zhu, T., Li, J., Ogata, S., & Yip, S. Mechanics of ultra-strength materials. MRS Bull. **34**, 167-172 (2009)

[11] Li, J., Van Vliet, K. J., Zhu, T., Yip, S., & Suresh, S. Atomistic mechanisms governing elastic limit and incipient plasticity in crystals. Nature **418**, 307-310 (2002)

[12] Schuh, C. A., Mason, J. K. & Lund, A. C. Quantitative insight into dislocation nucleation from high-temperature nanoindentation experiments. Nature Mater. **4**, 617, (2005)

[13] Schall, P., Cohen, I., Weitz, D. A. & Spaepen, F. Visualizing dislocation nucleation by indenting colloidal crystals. Nature **440**, 319-323 (2006).

[14] Xu, G., Argon, A. S., & Ortiz, M. Critical configurations for dislocation nucleation from crack tips. Philos. Mag. A **75**, 341-367 (1997).

[15] Bringa, E. M. et al. Shock deformation of face-centred-cubic metals on subnanosecond timescales. Nature Mater. **5**, 805-810 (2006).

[16] Tschopp, M. A., Spearot, D. E., & McDowell, D. L. Atomistic simulations of homogeneous dislocation nucleation in single crystal copper. Modelling Simul. Mater. Sci. Eng., **15**, 693-709 (2007).

[17] Zhu, T., Li, J., Samanta, A., Leach, A., & Gall, K. Temperature and strain-rate dependence of surface dislocation nucleation. Phys. Rev. Lett **100**, 025502 (2008).

[18] Vineyard, G. H. Frequency factors and isotope effects in solid state rate processes. J. Phys. Chem. Solids **3**, 121-127 (1957).

[19] Jónsson, H., Mills, G., & Jacobsen, K. W., Nudged elastic band method for finding minimum energy paths of transitions., in *classical and quantum dynamics in condensed phase simulations*, Ed. Berne, B. J., Ciccotti G. & Coker, D. F., 385-404 (World Scientific, 1998).

[20] Warner D. H. & Curtin, W. A., Origins and implications of temperature-dependent activation energy barriers for dislocation nucleation in face-centered cubic metals. Acta. Mater. **57**, 4267-4277 (2009).

[21] Frenkel, D. & Smit, B. *understanding molecular simulation: from algorithms to applications*, Academic Press, San Diego, (2002)

[22] Becker, R. & Döring, W. The kinetic treatment of nuclear formation in supersaturated vapors Ann. Phys. (N.Y.) **24**, 719-752 (1935).

[23] Khantha, M., Pope, D. P., & Vitek, V. Dislocation screening and the brittle-to-ductile transition: a Kosterlitz-Thouless type instability. Phys. Rev. Lett. **74**, 684-687 (1994).

[24] Mishin, Y., Mehl, M. J., Papaconstantopoulos, D. A., Voter, A. F., & Kress, J. D. Structural stability and lattice defects in copper: ab initio, tight-binding, and embedded-atom calculations. Phys. Rev. B. **63**, 224106 (2001)

[25] Hirth, J. P. & Lothe, J. *Theory of Dislocations* (Krieger, New York, 1992)

[26] Ryu, S. & Cai, W. Validity of classical nucleation theory for Ising models Phys. Rev. E, **81**, 030601 (R) (2010)

[27] Ngan, A. H. W., Zuo, L., & Wo, P. C. Size dependence and stochastic nature of yield strength of micron-sized crystals: a case study on Ni3Al. Proc. Royal Soc. A **462**, 1661-1681 (2006)

[28] Zeldovich, Y. B., On the theory of new phase formation: cavitation. Acta Physiochim. URSS, **18**, 1-22 (1943).

[29] Zhu, T., Li, J., Samanta, A., Kim, H. G., & Suresh, S. Interfacial plasticity governs strain rate sensitivity and ductility in nanostructured metals. Proc. Natl. Acad. Sci. USA **104**, 3031 (2007).

[30] Kemeny, G. & Rosenberg, B. Compensation law in thermodynamics and thermal death. Nature **243**, 400 (1970).

[31] Huntington, H. B., Shirn, G. A., & Wajda, E. S. Calculation of the entropies of lattice defects. Phys. Rev. **99**, 1085 (1955).

[32] DiMelfi, R. J., Nix, W. D., Barnett, D. M. & Pound, G. M. The equivalence f two methods for computing the activation entropy for dislocation motion. Acta. Mater. **28**, 231-337 (1980).

[33] Whalley, E. Use of volumes of activation for determining reaction mechanisms. in *Advances in Physical Organic Chemistry*, Gold, V. ed., 93-162, (Academic Press, London, 1964).

[34] Tonnet, M. L., & Whalley, E. Effect of pressure on the alkaline hydrolysis of ethyl acetate in acetone-water solutions. parameters of activation at constant volume. Can. J. Chem. **53** 3414-3418 (1975).

FIGURE LEGENDS

Figure 1 : (a) Schematics of the simulation cell. The spheres represent atoms enclosed by the critical nucleus of a Shockley partial dislocation loop. (b) Shear stress-strain curves of the Cu perfect crystal (before dislocation nucleation) at different temperatures.

Figure 2 : (a) Free energy of dislocation loop during homogeneous nucleation at T = 300 K, σ_{xy} = 2.16 GPa (γ_{xy} = 0.135) from umbrella sampling. (b) Size fluctuation of critical nuclei from MD simulations.

Figure 3 : Activation free energy for homogeneous dislocation nucleation in copper. (a) F_c as a function of shear strain γ at different T. (b) G_c as a function of shear stress σ at different T. Squares represent umbrella sampling data and lines represent zero temperature MEP search results using simulation cells equilibrated at different temperatures. (c) F_c as a function of T at $\gamma = 0.092$. Circles represent umbrella sampling data and dashed line represent a polynomial fit. (d) G_c as a function of T at $\sigma = 2.0$ GPa from polynomial fit.

Figure 4 : (a) Heterogeneous dislocation nucleation in a copper nanorod under compression. (b) G_c as a function compressive stress σ at different T. (c) Contour lines of dislocation nucleation rate per site I as a function of T and σ. The predictions with and without accounting for activation entropy $S_c(\sigma)$ are plotted in thick and thin lines, respectively. The nucleation rate of $I \sim 10^6 \mathrm{s}^{-1}$ per site is accessible in typical MD time scales while nucleation rate of $I \sim 10^{-4}$-10^{-9} is accessible in typical experimental time scales, depending on the number of nucleation sites.

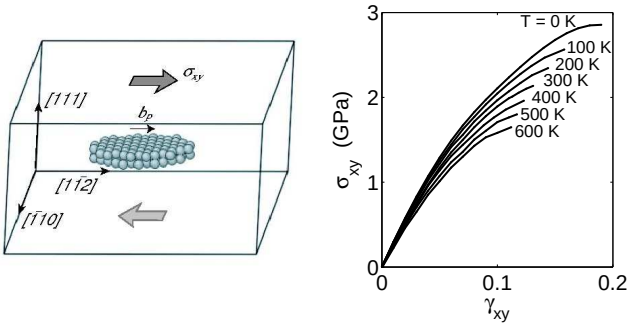
σ_{xy}
[111]
b_p
[11$\bar{2}$]
[$\bar{1}$10]
T = 0 K
100 K
200 K
300 K
400 K
500 K
600 K
σ_{xy} (GPa)
γ_{xy}
0
1
2
3
0
0.1
0.2

(a) (b)

FIG. 1:

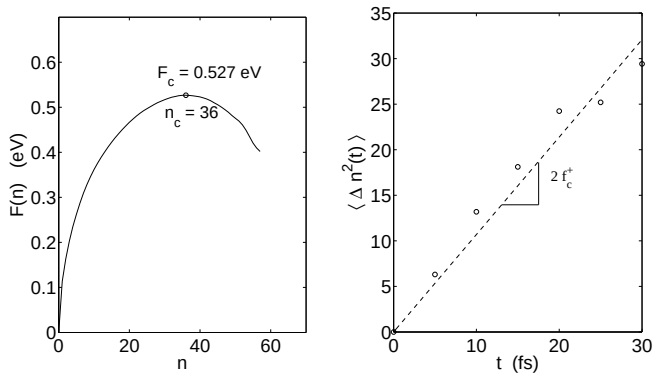

(a) (b)

FIG. 2:

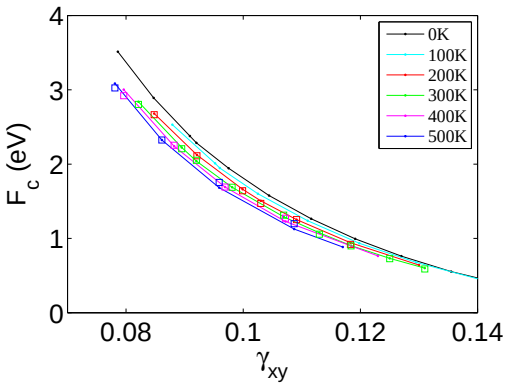
0K
100K
200K
300K
400K
500K
F_c (eV)
γ_xy

(a)

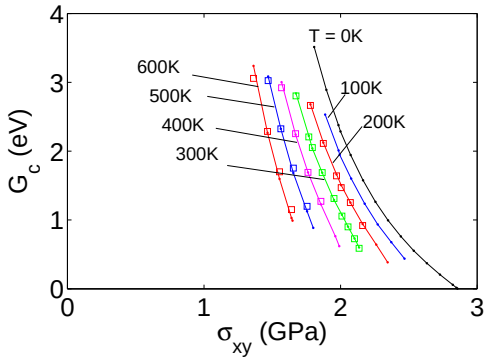
T = 0K
100K
200K
600K
500K
400K
300K
G_c (eV)
σ_xy (GPa)

(b)

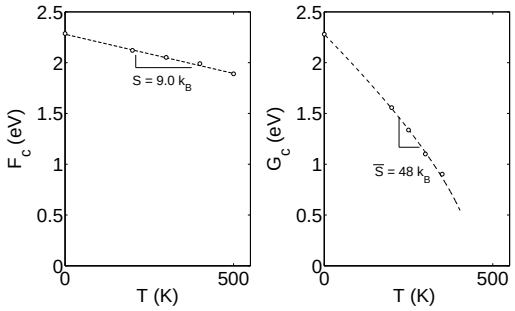
S = 9.0 k_B
F_c (eV)
T (K)
S = 48 k_B
G_c (eV)
T (K)

(c) (d)

FIG. 3:

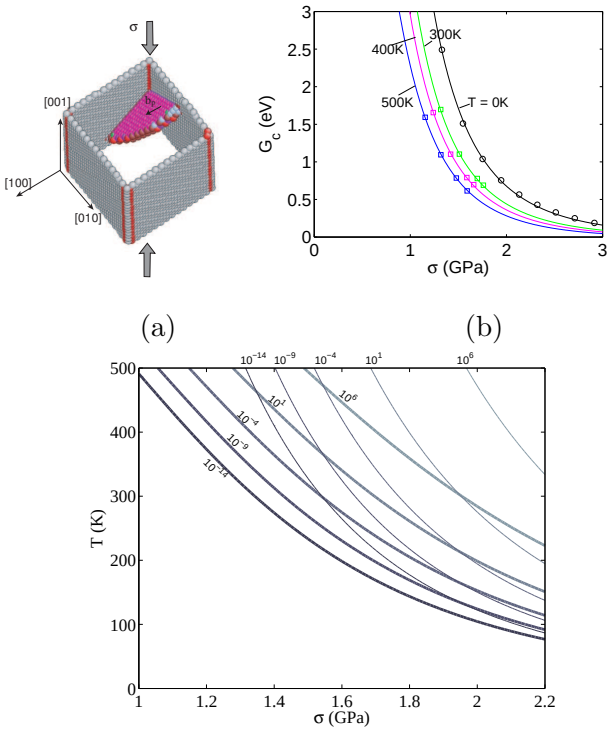
σ
[001]
[100]
[010]
b
(a)
G_c (eV)
σ (GPa)
400K
300K
500K
T = 0K
(b)
T (K)
σ (GPa)
10^{-14}
10^{-9}
10^{-4}
10^{1}
10^{6}
(c)

FIG. 4: